

Biased Orientation and Color Tuning of the Human Visual Gamma Rhythm

Ye Li,^{1,2} William Bosking,³ Michael S. Beauchamp,³ Sameer A. Sheth,^{1,2} Daniel Yoshor,³ Eleonora Bartoli,¹ and Brett L. Foster³

¹Department of Neurosurgery, ²Department of Neuroscience, Baylor College of Medicine, Houston, Texas 77030, and ³Department of Neurosurgery, Perelman School of Medicine at the University of Pennsylvania, Philadelphia, Pennsylvania 19104

Narrowband γ oscillations (NBG: \sim 20–60 Hz) in visual cortex reflect rhythmic fluctuations in population activity generated by underlying circuits tuned for stimulus location, orientation, and color. A variety of theories posit a specific role for NBG in encoding and communicating this information within visual cortex. However, recent findings suggest a more nuanced role for NBG, given its dependence on certain stimulus feature configurations, such as coherent-oriented edges and specific hues. Motivated by these factors, we sought to quantify the independent and joint tuning properties of NBG to oriented and color stimuli using intracranial recordings from the human visual cortex (male and female). NBG was shown to display a cardinal orientation bias (horizontal) and also an end- and mid-spectral color bias (red/blue and green). When jointly probed, the cardinal bias for orientation was attenuated and an end-spectral preference for red and blue predominated. This loss of mid-spectral tuning occurred even for recording sites showing large responses to uniform green stimuli. Our results demonstrate the close, yet complex, link between the population dynamics driving NBG oscillations and known feature selectivity biases for orientation and color within visual cortex. Such a bias in stimulus tuning imposes new constraints on the functional significance of the visual γ rhythm. More generally, these biases in population electrophysiology will need to be considered in experiments using orientation or color features to examine the role of visual cortex in other domains, such as working memory and decision-making.

Key words: color; gamma; human; orientation; oscillations; vision

Significance Statement

Oscillations in electrophysiological activity occur in visual cortex in response to stimuli that strongly drive the orientation or color selectivity of visual neurons. The significance of this induced “ γ rhythm” to brain function remains unclear. Answering this question requires understanding how and why some stimuli can reliably generate oscillatory γ activity while others do not. We examined how different orientations and colors independently and jointly modulate γ oscillations in the human brain. Our data show that γ oscillations are greatest for certain orientations and colors that reflect known response biases in visual cortex. Such findings complicate the functional significance of γ oscillations but open new avenues for linking circuits to population dynamics in visual cortex.

Introduction

Within visual cortex, high-frequency electrophysiological activity can be induced by visual stimulation. This induced ‘ γ ’ range (\sim 20–200 Hz) activity is composed of at least two distinct spectral responses: asynchronous broadband- or ‘high-’ γ (BBG; \sim 70–200 Hz) and oscillatory narrow-band γ (NBG; \sim 20–60 Hz) (Ray and Maunsell, 2011; Bartoli et al., 2019). NBG has been the subject of detailed experimental (Fries et al., 2007; Fries, 2009) and computational (Buzsaki and Wang, 2012) study, leading to a proposed role in synchronizing functional brain dynamics important for perception and cognition (Fries, 2015). While these efforts have shown that early reports of visual NBG activity can be replicated across species (Fries et al., 2008; Buzsaki et al., 2013), debate still surrounds its functional significance (Ray and

Received May 25, 2021; revised Nov. 19, 2021; accepted Dec. 15, 2021.

Author contributions: Y.L., E.B., and B.L.F. designed research; Y.L., W.B., M.S.B., S.A.S., D.Y., E.B., and B.L.F. performed research; Y.L. and E.B. analyzed data; Y.L. and E.B. wrote the first draft of the paper; Y.L., W.B., M.S.B., E.B., and B.L.F. edited the paper; Y.L., E.B., and B.L.F. wrote the paper.

This work was supported by National Institutes of Health Grants R01MH106700 and U01NS108923 to S.A.S., R01EY023336 to D.Y., and R01MH116914 to B.L.F. S.A.S. was also supported by the McNair Foundation and Dana Foundation. We thank Ping Sun, Denise Oswalt, Zhuokun Ding, and Jiayang Xiao for contributing to the receptive field data processing and visualization.

The authors declare no competing financial interests.

Correspondence should be addressed to Brett L. Foster at brett.foster@pennmedicine.upenn.edu or Eleonora Bartoli at eleonora.bartoli@bcm.edu.

<https://doi.org/10.1523/JNEUROSCI.1085-21.2021>

Copyright © 2022 the authors

Maunsell, 2015). Specifically, debate has focused on the stimulus dependence of visually induced NBG (Brunet et al., 2014; Hermes et al., 2015a). Despite longstanding evidence (Kayser et al., 2003, 2004), it is now clear that standard grating or Gabor patch stimuli are particularly suited at inducing NBG. In contrast, more complex stimuli (e.g., natural images) often fail to evoke robust NBG responses (Kayser et al., 2003; Hermes et al., 2015b; Bartoli et al., 2019). Furthermore, the magnitude and peak frequency of NBG are sensitive to grating attributes, such as size (Gieselmann and Thiele, 2008; Jia et al., 2011), contrast (Ray and Maunsell, 2010; Bartoli et al., 2019), and spatial frequency (Jia et al., 2011; Dubey and Ray, 2020). Recently, it has also been shown that visual NBG can be induced by color stimuli, with a predominate preference for long wavelengths (i.e., red/orange) (Shirhatti and Ray, 2018; Bartoli et al., 2019). Interestingly, γ responses to grating or uniform color stimuli are contextually modulated by discontinuities between the receptive field (RF) and surround (Vinck and Bosman, 2016; Peter et al., 2019). This dependence on structural and chromatic stimulus features can account for difficulties in predicting which complex stimuli will evoke NBG oscillations (Brunet et al., 2014, 2015; Hermes et al., 2015a,b; Bartoli et al., 2019, 2020).

While the circuits processing orientation and color have historically been viewed as having modest overlap, this is a simplified dichotomy. Neurons in visual cortex show complex tuning properties to orientation and color stimuli (Leventhal et al., 1995; Economides et al., 2011). Furthermore, recent cellular imaging work in the nonhuman primate has provided clear evidence for joint orientation and color tuning by neurons in early visual cortex (Garg et al., 2019). This joint tuning suggests that activation of overlapping circuits may account for the structural and chromatic tuning of visual γ (Bartoli et al., 2020). To date, it is unknown how color and orientation jointly influence the emergence of γ oscillations in visual cortex. However, recent work has shown that visual γ is sensitive to incongruous center-surround attributes for both color or orientation stimuli (Peter et al., 2019; Shirhatti et al., 2020; Uran et al., 2020). Therefore, visual γ rhythms can be modulated by specific stimulus configurations uniformly driving features strongly represented in the locally recorded population, whereby NBG provides a partial readout of underlying large-scale circuit properties, such as population tuning bias for some stimulus features (Bartoli et al., 2020). If correct, the visual γ rhythm should display a dependence and tuning profile similar to prior observations of such population tuning biases in early visual cortex. Indeed, evidence from the nonhuman primate suggests that visual γ displays putative cardinal orientation tuning (Dubey and Ray, 2020), a bias in population tuning also observed in human visual cortex through neuroimaging (Furmanski and Engel, 2000; Sun et al., 2013). Also, the chromatic tuning of visual γ shows some correspondence to previously reported end-spectral biases (i.e., stronger responses to red and blue) in early visual cortex (Nasr and Tootell, 2018). Crucially, orientation tuning of γ has yet to be systematically examined with direct recordings in the human brain, and no previous study has addressed how this tuning relates to color nor the joint tuning of orientation and color.

To address these questions, we performed intracranial recordings from human early visual cortex to quantify orientation, color, and joint orientation-color tuning of the visual NBG rhythm. Across four experiments, we observed NBG to display cardinal orientation bias, as well as both end- and mid-spectral color biases. Interestingly, when jointly driving orientation and

Table 1. Subject information^a

Subject	Age (yr)	Sex	Hemisphere	Electrode type	Visual areas				Experiments				
					N _{Occ}	N _{VEP}	V1	V2	V3	V4	E1	E2	
N1	41	F	L	ECoG	31	30	25	3	0	0	Yes	—	Yes
N2	22	M	B	ECoG	12	6	5	1	0	0	—	Yes ^b	Yes Yes ^b
N3	33	F	R	sEEG	22	14	8	2	1	0	Yes	Yes	Yes
N4	34	F	L	sEEG	12	3	0	0	0	1	—	Yes	—
N5	39	M	L	sEEG	26	24	6	1	2	3	—	Yes ^b	—
N6	36	F	L	sEEG	10	7	1	3	0	0	Yes	Yes	Yes Yes
N7	53	F	L	sEEG	8	8	5	0	1	0	Yes	Yes	Yes Yes
Total					121	92	50	10	4	4			

^a Demographic information, hemispheric implanted (L, left; R, right, B, bilateral), and count of electrodes in occipital lobe (N_{Occ}). Electrodes used in the main analyses were selected by means of a functional criterion (displaying a VEP). We further assigned the electrodes to different visual areas (V1-V4) based on a probabilistic cytoarchitectonic atlas (vcAtlas) (Rosenke et al., 2018) as previously described (Bartoli et al., 2019). Some electrodes were not assigned to any visual area.

^b For experiment participation, a subset of the orientations were recorded (4 in place of 8 orientations). E1, Static grating task; E2, drifting grating task; E3, uniform color task; E4, color grating task.

color, cardinal orientation and mid-spectral color tuning were attenuated while end-spectral bias was maintained. These findings suggest a striking relationship between visual γ tuning and recent observations about the distribution of orientation and color tuning within visual cortex (Garg et al., 2019; Liu et al., 2020). This tight link between functional circuit properties and visual γ tuning provides a fruitful avenue for bridging scales of organization while providing important constraints and new directions for the functional significance of γ oscillations in vision and cognition.

Materials and Methods

Human subjects

Seven subjects (N1-N7; 2 males, mean age 37 years, range 22–53 years) were included in this study. All subjects were being monitored with invasive neural recordings (electrocorticography [ECoG] in N1 and N2; stereo-EEG [sEEG] in N3-N7) for the potential surgical treatment of refractory epilepsy at Baylor St. Luke's Medical Center. Detailed subject information is reported in Table 1. All subjects participated in this study with both written and verbal consent, completing at least one task in our experimental inventory. Experimental procedures were in accordance with the policy and principles contained in the Declaration of Helsinki and were approved by the Institution Review Board at Baylor College of Medicine (IRB Protocol H-18112). No patients with epileptic foci, anatomic abnormalities, or prior surgical resection in posterior regions participated in this study. Experiments were recorded while interictal epileptic discharges were absent in the areas of interest. We note that part of the data recorded from Subject N1 (Experiment 3: uniform color) was previously reported by Bartoli et al. (2019) under the subject identification code N10. No other datasets from the current study have been previously reported.

Electrode arrays

Reported data were acquired by ECoG electrode arrays in 2 subjects (N1 and N2) and sEEG depth probes in the remaining 5 subjects (N3-N7). The subdural array implanted in Subject N1 was custom-designed by PMT to incorporate a high-density electrode mini grid (4 × 6; 0.5 mm diameter) into a standard macro-ECoG (1 × 8 electrodes with 3 mm diameter) linear array configuration (Bosking et al., 2017; Bartoli et al., 2019). Macro electrodes incorporating the mini grid have an 18 mm center-to-center distance, while other macro electrodes in the array have 10 mm distance. The interhemispheric grid (2 × 8) array implanted in Subject N2 had dual-sided electrode contacts, with 4 mm diameter and 10 mm center-to-center distance (Ad-Tech Medical Instrument). Depth sEEG electrodes in Subjects N3-N7 had a 0.8 mm diameter, with 8-16 contacts along the probe with a 3.5 mm center-to-center distance (PMT). Detailed electrode information for each subject is reported in Table 1.

Electrode localization and selection

For each subject, we determined electrode locations by using the software pipeline iELVis (intracranial Electrode Visualization) (Groppe et al., 2017). In short, the postoperative CT image was registered to the pre-operative T1 anatomic MRI image using FSL (Jenkinson et al., 2012). Next, the location of each electrode was identified in the CT-MRI overlay using BioImage Suite (Papademetris et al., 2006). For subdural (ECoG) electrodes, coordinates were adjusted for brain shifts by projecting the electrode array to the cortical surface model, reconstructed from the T1 image using Freesurfer (version 5.3) (Dale et al., 1999). For depth sEEG electrodes, no location correction was used. For the hybrid mini-macro subdural electrode array in N1, mini-ECoG electrode coordinates were calculated by custom functions combining the macro-ECoG coordinates with the known array geometry.

To identify electrodes in “visual” cortex, we applied an electrode selection criterion previously reported by Bartoli et al. (2019). Briefly, electrodes of interest were those localized within the occipital lobe, with the following anatomic boundaries: (1) dorsal: the parieto-occipital sulcus; (2) ventral: the lingual gyrus; and (3) dorsolateral: the trans-occipital sulcus and posterior aspect of the superior temporal sulcus. Using these criteria, we identified 121 electrodes within the occipital cortex from all 7 subjects (range 8–31 electrodes within each subject). We further assigned each electrode to fall within a subdivision of visual occipital areas (V1–V4) by mapping the cytoarchitectonic atlas vcAtlas (<http://vpnl.stanford.edu/vcAtlas>) (Rosenke et al., 2018) onto each individual cortical surface using Freesurfer. The distribution of electrodes in four subdivisions is reported in Table 1. Occipital electrodes were further selected by means of a functional response criterion (see Visually responsive electrode identification). To visualize electrodes of interest on a common brain, we transformed electrode coordinates into the MNI305 space and represented them as spheres on the Freesurfer fsaverage brain (see Fig. 1).

Experimental design

All subjects performed at least one of the following visual experiments (for participation details, see Table 1) at the bedside in a quiet patient room. All tasks were presented on an adjustable monitor (1920 × 1080 resolution, 47.5 × 26.7 cm screen size, connected to a PC running Windows 10 Pro for Subjects N2, N6, and N7 and to an Apple iMac running OSX 10.9.4 for Subjects N1, N3–N5) at a viewing distance of 57 cm (such that 1 cm = ~1 deg visual angle). Tasks were programmed using Psychtoolbox-3 functions (version 3.0.16) (Brainard, 1997) running on MATLAB (R2019a, The MathWorks).

Experiment 1: static grating. Four subjects (N1, N3, N6, and N7) performed the full screen static grating task (see Fig. 2), which was previously described by Bartoli et al. (2019) (named as “visual grating task”). During the task, full screen static grayscale grating stimuli were presented for 500 ms, with a random interstimulus interval (ISI) between 1500 and 2000 ms. Stimuli of this task were sine wave gratings at three levels of Michelson contrast (20%, 50%, and 100%), and two orientations (0° and 90°). Each block of the static grating task included 105 trials in total, with 90 randomly presented stimulus trials of the 6 conditions (3 contrast levels × 2 orientations, 15 trials for each combination) and 15 target trials presenting 45° gratings at three contrast levels (5 trials for each). One block of the static grating task lasted around 4 min. Subjects were required to maintain fixation on a white cross at the screen center and respond via button press when a target stimulus occurred. Data from target trials was not included in further analyses.

Experiment 2: drifting grating. In the drifting grating task, 6 participants (Subjects N2–N7) were shown full screen moving grayscale grating stimuli (see Fig. 2). Grating stimuli had a sine wave spatial frequency of 1 cycle/degree and moved at the speed of 2 degree/s in two possible directions, orthogonal to the grating orientation. The spatial and temporal frequency settings were chosen to maximize V1/V2 responses (Henriksson et al., 2008; Dubey and Ray, 2020). Stimuli were presented for 500 ms with a random ISI between 1500 and 2000 ms. Stimuli in this task reflected three levels of Michelson contrast (20%, 50%, and 100%) across eight orientations (0°–157.5° with a 22.5° interval). All eight orientations were covered by two experimental runs: odd blocks contained 0°,

45°, 90°, and 135° stimuli, while even blocks contained 22.5°, 67.5°, 112.5°, and 157.5° stimuli. Each block of the drifting grating task included 240 randomly presented stimuli from the 12 conditions (three contrast levels × four orientations, 20 trials for each condition), lasting ~10 min. N2 and N5 only completed one block of the drifting grating task and do not have data on orientations of 22.5°, 67.5°, 112.5°, and 157.5°. Group analyses adjust for this factor. During the task, subjects were required to maintain fixation on a green dot at the center of the screen and press a key when the fixation dot changed size (the fixation dot varied from a 40 pixel diameter to 30 pixel diameter, on one-third of the trials). Dot size changed during the 150–450 ms time window after stimulus onset. Data from all trials were included in the analysis. Mean task accuracy was 92.7%.

Experiment 3: uniform color. Five subjects (N1–N3, N6, and N7) performed a full screen uniform color task, which was previously described by Bartoli et al. (2019) (named as “visual color task”). Full screen uniform colors (red, orange, yellow, green1, green2, blue1, blue2, purple, gray, and white; see Fig. 4) were presented for 500 ms with a random ISI between 1500 and 2000 ms. Color space and luminance values are shown in Table 2. Subjects were required to maintain fixation on a white cross at the center of the screen and press a key when the target color (white) was presented. Each block of the uniform color task randomly presented 140 stimuli (15 trials for each color, 5 trials for target white), lasting ~5 min.

Experiment 4: color grating. In the color grating task, 4 participants (N2, N3, N6, and N7) were shown full screen chromatic moving grating stimuli (see Fig. 5). Grating spatial frequency, velocity, and duration parameters were identical to Experiment 2. Gratings were composed of one color (either red, green, blue) against a gray background across eight orientations (0°–157.5° with a 22.5° interval). Colors were selected to match the luminance of the gray background and to have a similar color setting with respect to previous studies (see Table 2) (Garg et al., 2019; Peter et al., 2019). Therefore, the colors used in Experiment 4 are different from the colors used in Experiment 3. However, we note that the green used in Experiment 4 is very similar to green2 in Experiment 3 with minor saturation adjustments. More details are provided in Control analyses for luminance and chromaticity. Similar to the drifting grating task, each block of the color grating task randomly presented 240 stimuli from 12 conditions (3 colors × 4 orientations, either 0°–135° with 45° intervals or 22.5°–157.5° with 45° intervals, 20 trials for each condition), lasting ~10 min. Two blocks of different orientation settings were required to show all 8 orientations (N2 only completed one block of the color grating task and does not have data on orientations of 22.5°, 67.5°, 112.5°, and 157.5°). Subjects were required to maintain fixation on a white dot at the center of the screen and press a key when the dot changed size (see details from Experiment 2). Mean task accuracy was 90%.

Electrophysiological recording

ECoG and sEEG signals were recorded by a 256 channel BlackRock Cerebus system (BlackRock Microsystems) at 2 kHz sampling rate, with a fourth-order Butterworth bandpass filter of 0.3–500 Hz. ECoG recordings were referenced to an inverted (facing the dura) subdural intracranial electrode, sEEG recordings were referenced to an electrode contact visually determined to be located outside of gray matter. A photodiode sensor recording at 30 kHz was attached to the task monitor to synchronize intracranial recordings to the stimulus presentation.

Data analysis: preprocessing and spectral decomposition

All signals were processed by custom scripts in MATLAB (R2019a, The MathWorks). Raw EEG signals were first inspected for line noise, recording artifacts, and interictal epileptic spikes. Electrodes with artifacts and epileptic spikes were excluded from further analysis. Next, each channel was notch filtered (60 Hz and harmonics) and rereferenced to the common average of all selected electrodes. Finally, all rereferenced signals were downsampled to 1 kHz and spectrally decomposed using a family of Morlet wavelets, with center frequencies ranging linearly from 2 to 200 Hz in 1 Hz steps (7 cycles).

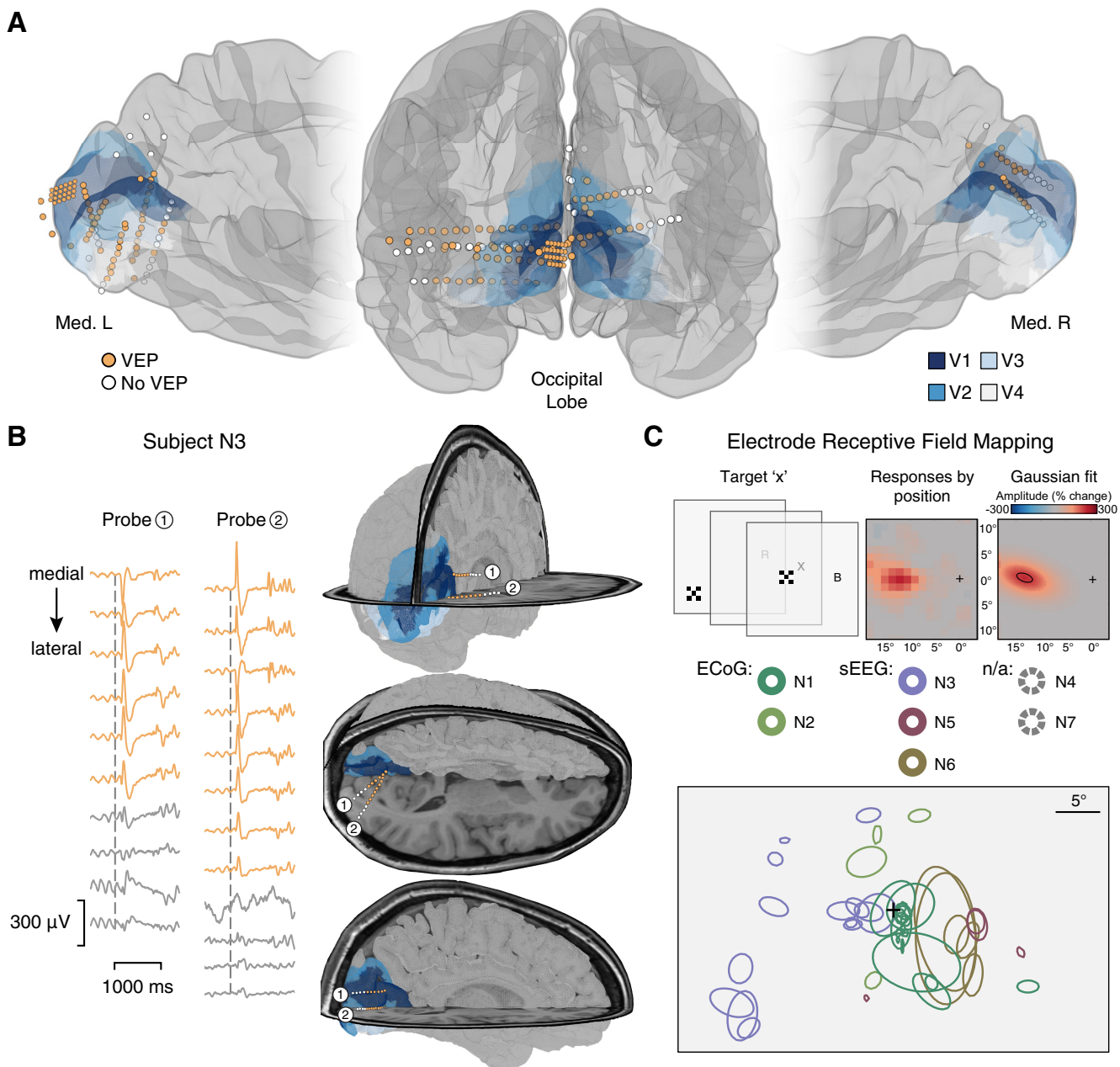


Figure 1. Recording sites within visual cortex and RF mapping. **A**, Anatomical location of electrodes from all subjects participating in the current study on a standard cortical surface (see Materials and Methods). Orange represents VEP electrodes ($n = 92$). White represents non-VEP ($n = 29$) electrodes. V1-V4 areas from the vcAtlas are mapped onto the standard cortical surface (see Materials and Methods). **B**, Anatomical location of electrodes from an sEEG case (Subject N3). Inset, The mean voltage traces for each electrode of two probes targeting visual cortex. Orange represents sites and traces of VEP identified electrodes. **C**, RF mapping procedure for the left hemifield (see Materials and Methods) and depiction of electrode RFs ($n = 48$) relative to fixation on the screen (RF mapping not performed in N4 and N7).

Visually responsive electrode identification

Visually responsive electrodes were identified based on the presence of a visual evoked potential (VEP) to grating stimuli, following the definition from a previous study (Bartoli et al., 2019). This functional criterion was used to exclude electrodes lacking a robust visual response and at the same time to avoid circularity by focusing on an independent signal feature with respect to the one of interest (i.e., NBG). Electrodes localized within the occipital lobe were defined as “responsive” if: (1) the voltage standard deviation (SD) for the response window (0–250 ms) was at least 3 times greater than the SD for the baseline window (−1000 to 0 ms); and (2) the voltage range for the response window was at least 10 times larger than the SD for the baseline window. The electrodes selected based on the presence of a VEP were 76% of the electrodes localized to the occipital lobe across all subjects (92 of 121 electrodes). More than 50% of

the visually responsive electrodes were localized in V1 (50 of 92). Only VEP electrodes were further selected and analyzed (see below). Additional details for each subject are listed in Table 1 and in Figure 1.

Statistical analyses

Statistical analyses primarily focused on changes in NBG signal properties across task conditions. NBG amplitude was obtained via averaging the magnitude of the Morlet wavelet decomposition result (2-200 Hz in 1 Hz steps, 7 cycles) between 20 and 60 Hz. Amplitude values were normalized to percent change with respect to the prestimulus baseline period (500 ms before stimulus onset). As described below, different statistical tests were used to appropriately evaluate the effects of interest for each analysis. Primarily, multilevel mixed-effects models were adopted to account for the unbalanced and nested data structure in the

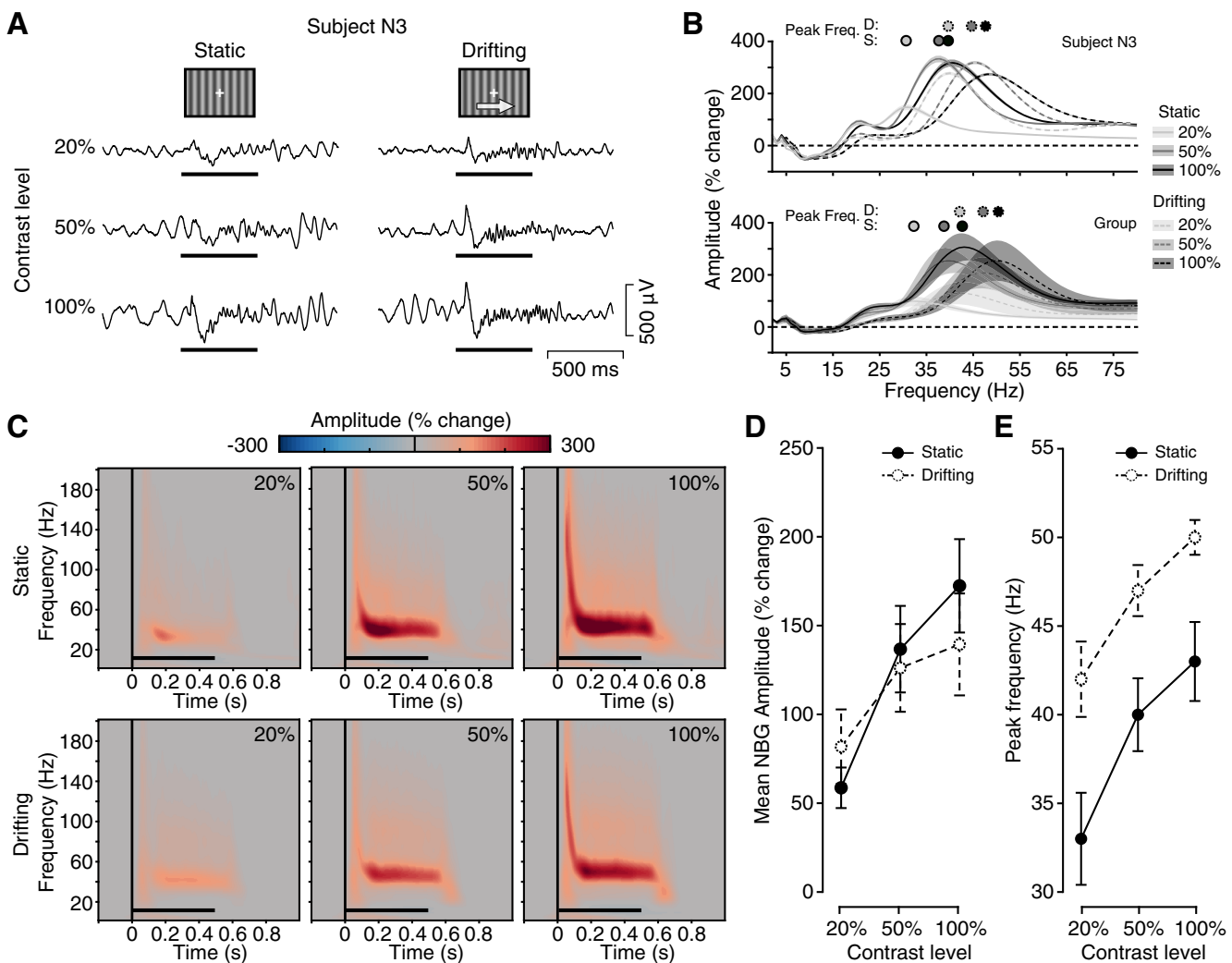


Figure 2. Experiments 1 and 2: spectral response to static and drifting grating stimuli. **A**, Example single-trial voltage responses (from Subject N3) for each contrast level in Experiments 1 and 2. Grating stimuli were presented for 500 ms (black horizontal line), with a random ISI of 1.5–2.0 s. Drifting grating motion was in one of two orthogonal directions for each trial (directions balanced across trials). **B**, Normalized amplitude spectra (from all VEP electrodes) for each contrast level in Experiments 1 and 2 averaged from the 250–500 ms poststimulus time window, shown for an example Subject N3 (top) and group mean (bottom; n elecs = 59 for Experiment 1, n elecs = 62 for Experiment 2). Filled circles represent peak amplitude frequency (D, drifting grating; S, static grating). Shading represents SE. The peak frequency of NBG monotonically increases for higher grating contrast levels in both tasks. **C**, Group-average spectrograms for each grating contrast level in Experiment 1 (from Subjects N1, N3, N6, and N7; n elecs = 59) and Experiment 2 (from Subjects N2–N7; n elecs = 62). Color maps represent percentage change in amplitude relative to the prestimulus period (−500 to 0 ms). Black horizontal line indicates stimulus presentation. **D**, Group-average mean NBG amplitude in Experiments 1 and 2 (average of Subjects N3, N6, and N7, who completed both experiments; n elecs = 29). Error bar indicates ± 1 standard error (SE). **E**, Group-average NBG peak frequency in Experiments 1 and 2 (average of Subjects N3, N6, and N7, who completed both experiments; n elecs = 29). Error bar indicates ± 1 SE. While both tasks induce monotonic increases in NBG peak frequency across contrast levels, drifting gratings induce substantially faster peak frequencies across all contrasts levels.

current study (i.e., multiple electrodes from each subject), such that experimental conditions (e.g., contrast level) were set as fixed effects whereas subjects and electrodes were set as nested random effects. To evaluate the importance of a fixed effect, the model was compared with a simpler model without the coefficients of interest but with identical random effects structure (Bates et al., 2015). This approach accounts for the nonindependence between observations (e.g., different electrodes from the same subject) while preserving the richness of the dataset (e.g., avoiding averaging across electrodes).

Effect of contrast level and grating motion

To quantify how the amplitude and peak frequency of induced NBG were modulated by the contrast level in Experiments 1 and 2, we computed the log-transformed NBG peak amplitude (to correct for skewness) and NBG peak frequency at the single-trial level. We used mixed-effects models to evaluate the effect of contrast on NBG amplitude and peak frequency (*lme4* library) (Bates et al., 2014) in R (R Development Core Team, 2010). We modeled contrast level as a fixed effect, and

electrodes and subjects as nested random effects (i.e., full model). To evaluate the impact from the stimulus contrast, we compared the full model to a reduced model with the same random effect structure but no fixed effect (only an intercept term to capture the average). In Results, we report the *p* value of the model comparison, assessing the significance of the fixed effect.

To further test whether the amplitude and peak frequency of induced NBG were modulated by the grating motion (i.e., static vs drifting), we combined the data from Experiments 1 and 2, and we modeled both the grating motion and contrast level as fixed effects, using the same nested random effect structure as described above (i.e., full model). By comparing this model with a reduced model (without motion as a fixed effect), we were able to evaluate the importance of grating motion while accounting for contrast. In Results, we report the p value of the model comparison. The interaction between grating motion and contrast level on mean log NBG amplitude was tested by comparing a model with the additional interaction term to the full model above.

Table 2. Color space coordinates (RGB and CIE Lxy) and luminance values of all color stimuli in Experiments 3 and 4^a

	RGB			CIE Lxy		Luminance (cd/m ²)
	R	G	B	x	y	
Experiment 3						
Gray	119	119	119	0.28	0.26	19.43
Red	232	0	122	0.41	0.21	19.22
Orange	215	66	18	0.56	0.36	18.60
Purple	161	80	217	0.23	0.13	21.31
Blue-1	0	128	255	0.17	0.13	21.31
Blue-2	0	146	215	0.18	0.17	26.26
Green-1	0	147	117	0.22	0.31	21.45
Green-2	0	139	0	0.30	0.59	17.09
Brown	145	116	0	0.46	0.47	18.13
Experiment 4						
Gray	80	80	80	0.28	0.26	9.26
Red	160	0	0	0.60	0.32	7.78
Green	0	97	0	0.30	0.58	8.60
Blue	0	65	180	0.16	0.10	9.39

^aPrestimulus background color is the same gray used in each experiment, respectively.

Permutation tests were used for *post hoc* comparisons of the grating motion effect at each contrast level. To balance the trial number from each task at a given contrast level, we randomly selected trials from the drifting grating task with the same trial number in the static grating task. Then, the condition labels were shuffled and the difference of NBG peak frequency between the two tasks was calculated for each contrast level. By repeating this process 10,000 times, null distributions of differences at three contrast levels were built. The exact *p* value for each contrast-level comparison was calculated by the rank of the original difference in the null distribution. To adjust for multiple comparisons, we used a Bonferroni-corrected significance level, reported in Results as *p*_{corr}.

Orientation tuning

To quantify orientation tuning of NBG amplitude in Experiments 2 and 4, we computed an orientation selectivity vector for each VEP electrode using the following formula:

$$\text{Orientation selectivity vector} = \frac{\left| \sum_{i=1}^N R_i e^{(j \cdot 2\theta_i)} \right|}{\sum_{i=1}^N R_i}$$

Where θ_i and R_i reflect orientation and NBG amplitude, respectively. The NBG amplitude values were scaled by the maximum value across all orientations to range between 0 and 1 for each electrode. Half the angle of the orientation selectivity vector represents the preferred orientation for a given electrode, while the magnitude of the vector represents the orientation selectivity strength.

We used circular mixed-effect models (Cremers and Klugkist, 2018) to evaluate the contrast effect and color effect on the preferred orientation of VEP electrodes (bpnreg library in R) (Cremers, 2020). The contrast level (or color) was modeled as the fixed effect, while subjects and electrodes were modeled as nested random effects. A significant difference between conditions would be indicated by nonoverlapping 95% highest posterior density intervals. In addition, linear mixed-effect models were used to evaluate the contrast effect and color effect on the orientation selectivity strength, similar to what was reported in the previous section. Last, we aimed at comparing orientation tuning between Experiments 2 and 4 (achromatic and chromatic gratings), to evaluate whether the presence of color modulated the preferred orientation (preferred angle) and/or the orientation selectivity strength (between 0 and 1). To test the preferred orientation, we compared a linear mixed-effects model accounting for the interaction between grating orientation and experiment type with a simpler model lacking the interaction term (same random effect structure with electrodes nested within subjects). To compare the orientation selectivity strength, we used nonparametric

permutation testing by swapping the labels between the two drifting grating experiments (10,000 times).

Color tuning

Previous studies reported that NBG amplitude displays color tuning, especially for reddish hues. To replicate previous findings, we analyzed the average NBG amplitude values in response to different colors in Experiment 3 using a nonparametric Friedman test of differences as previously described (Bartoli et al., 2019). Permutation tests were used to compare the NBG amplitude values of hues to the chance group level (shuffling all the color labels within each subject 10,000 times) and electrode level (shuffling the color labels across all trials for each electrode 10,000 times). The *p* value was calculated by the rank of the original NBG amplitude values in the null distribution.

Given that two types of recording electrodes (i.e., ECoG and sEEG) were used, which sampled different visual areas (V1–V4), we used linear mixed-effects models to evaluate if the electrode type or visual area (grouped as V1 vs V2–V4) influenced the NBG color tuning response. We compared three models of NBG responses: a complex model with a three-way interaction between color, electrode type, and visual area was compared with a simpler model where the visual area coefficients were dropped (color by electrode type). This model was compared with an even simpler model where also the electrode type terms were dropped (only color was present as a fixed effect). The three models had identical random effects structure, with electrodes nested in subjects.

Control analyses for contrast level and grating motion effects

To initially assess the influence of grating contrast and motion (static vs drifting), grating direction of motion and orientation were collapsed. To evaluate whether these two variables would additionally affect how contrast and grating motion modulate NBG amplitude and peak frequency, two control analyses were used.

First, data from Experiment 2 (drifting grating) were separated by direction, and the same modeling as above was used. No clear differences were observed in models using different sub-datasets. For each grating direction, the effect of contrast was significant for both NBG amplitude and NBG peak frequency (all *p*_{corr} < 0.05). Similarly, when testing for static versus drifting gratings separately for grating direction, both NBG amplitude and NBG peak frequency displayed the same pattern as in the main analysis when the grating directions were collapsed (all *p*_{corr} < 0.05).

In the second control analysis, we selected trials at 0° or 90° orientation from the drifting grating task to match the orientations in the static grating task. Results were similar when only trials at 0° or 90° orientation were used. Again, the main effects of contrast and grating motion for both NBG amplitude and NBG peak frequency were significant (all *p*_{corr} < 0.05). In summary, NBG peak amplitude and frequency are modulated by contrast levels and by grating motion in a similar fashion when considering different grating orientations and different directions of motion.

Control analyses for luminance and chromaticity

CIELxy coordinates of the stimuli presented in Experiments 3 and 4 were measured using a spectrophotometer (X-Rite i1 Pro, X-Rite). Stimulus luminance in Experiment 3 was greater (~20 cm²) (for more details, see Bartoli et al., 2019) than Experiment 4 (red: 7.8 cd/m², green: 8.6 cd/m², blue: 9.4 cd/m², gray: 9.3 cd/m²). To test whether the luminance or other chromatic differences might be affecting the observed results, we evaluated whether the mean NBG values obtained in response to each color stimulus in Experiment 3 and Experiment 4 displayed a dependence on CIELxy values measured using multiple regression. We found that the pattern of NBG tuning reported did not depend on luminance values (*p* = 0.12), or the *x* coordinate (*p* = 0.19) or the *y* (*p* = 0.29) of CIELxy color space. Therefore, the pattern of color tuning and color-orientation tuning reported in the main analyses cannot be explained by variations in color stimulus luminance settings or by chromatic coordinates in CIELxy space. Color and luminance values for Experiments 3 and 4 are shown in Table 2.

RF mapping

Five subjects (N1, N2, N3, N5, and N6) performed an RF mapping procedure (see Fig. 1C) (Yoshor et al., 2007). A black and white checkerboard was flashed at different screen locations (size = 3°, rate = 3 Hz) to sample the visual field, while the participant maintained central fixation and performed an oddball detection task (detect target “x” among a stream of letters presented at fixation; rate = 6 Hz). Each visual field location was sampled 12–15 times in random order. The visual field examined was dependent on electrode placement (i.e., relevant hemifield and eccentricity). For all subjects, the checkerboard locations were arranged in a grid with 3 degree spacing and spanned a minimum of 18° vertically and 18° horizontally. Mean BBG amplitude change was used to quantify the response of each electrode to a given checkerboard location. RF location and size were computed by interpolating responses across the checkerboard locations and fitting a 2D Gaussian as previously described (Yoshor et al., 2007). To exclude electrodes lacking a well-defined RF, fits with an $R^2 < 0.5$ were discarded. Electrode RFs for the 5 subjects (48 electrodes) are depicted relative to fixation in Figure 1C. Two control analyses were performed employing data from the RF mapping procedure and Experiment 1 (N1, N2, N6): (1) correlation between RF size and average NBG amplitude ($r = -0.41, p = 0.009$); and (2) RF size and NBG amplitude modulation by contrast ($r = -0.32, p = 0.04$). While a complete assessment of the influence of RF characteristics is beyond the scope of the current manuscript, we note that electrodes with smaller RFs (either because of smaller electrodes size or to the cortical location) tend to exhibit stronger γ oscillations as well as stronger modulations when considering static gratings. However, our ability to assess subtle changes in RF size across different visual areas or at different eccentricities within the same area is restricted because of the large size of the mapping stimulus that was used in the mapping procedure (3°). Future studies will be needed to precisely evaluate the relationship between NBG modulations and RF characteristics.

Results

Visual electrode identification

We used ECoG and sEEG recordings from human visual cortex in 7 subjects being invasively monitored for the potential surgical treatment of refractory epilepsy (Table 1). Across subjects, we obtained 121 electrodes within anatomically defined occipital cortex (Fig. 1A; for details, see Table 1). To exclude electrodes lacking robust visual responses from our analysis, we further applied a functional criterion to define visual responsiveness based on the presence of a VEP in response to a grating stimulus. As shown in Figure 1B, clear voltage deflections are observed after stimulus onset in VEP electrodes. In addition, we assigned each electrode to putative functional subdivisions of visual cortex using a probabilistic atlas (V1–V4, see Materials and Methods). Of all the electrodes within visual cortex, ~76% displayed a VEP (92 of 121). Of all VEP electrodes, 50 were within V1, 18 were within V2/V3/V4, and 24 were outside of V1–V4 (Table 1).

Peak frequency of induced NBG is increased for drifting versus static grating contrast

A large and growing literature shows visual grating stimuli to be particularly effective at inducing NBG activity (Ray and Maunsell, 2011; Hermes et al., 2015b; Bartoli et al., 2019). Consistent with this literature, we recently reported a strong positive correlation between grating contrast level and induced NBG peak frequency in human visual cortex (Bartoli et al., 2019). In the current study, we sought to use drifting grating stimuli, which are particularly effective at driving robust responses in early visual cortex.

To provide a bridge with our prior observations, we first replicated the grating contrast dependence of NBG responses for static stimuli. In addition, as we previously used invasively

implanted surface ECoG electrodes to measure visual NBG responses, the present replication served to ensure that similar effects were captured with sEEG depth electrodes. We therefore examined the amplitude and peak frequency of induced NBG as a function of contrast for both static and drifting grating stimuli. In Experiment 1 (static grating task), 4 subjects (N1, N3, N6–7) were presented with full-screen static grayscale gratings at three contrast levels (20%, 50%, and 100%; spatial frequency 1 cycle/degree), for a 500 ms duration. In Experiment 2 (drifting grating task), 6 subjects (N2–N7) were presented with full-screen drifting grayscale gratings at three contrast levels (20%, 50%, and 100%; spatial frequency 1 cycle/degree; velocity 2 degree/s), for a 500 ms duration.

Consistent with prior studies, we observed clear induced oscillatory responses in the raw voltage during both static and drifting grating presentation (Fig. 2A). As mentioned above, NBG amplitude and peak frequency are sensitive to the contrast level of static gratings (Ray and Maunsell, 2010; Hadjipapas et al., 2015; Bartoli et al., 2019). To replicate this finding in the current study, we computed the normalized amplitude spectra of the 250–500 ms poststimulus time window for the static grating task. As shown for a representative subject (N3) and at the group level in Figure 2B, the peak frequency of NBG monotonically increases for higher grating contrast levels. Similar results were found in the drifting grating task when calculating the normalized amplitude spectra for each contrast condition by averaging across other conditions (i.e., orientations and motion directions). Group-averaged spectrograms for both tasks show a similarly sustained NBG response during stimulus presentation (Fig. 2C), in addition to large transient BBG responses at stimulus onset, closely matching prior studies (Ray and Maunsell, 2010; Bartoli et al., 2019). Indeed, both tasks showed qualitatively similar increases in NBG amplitude across contrast levels (Fig. 2D). However, as shown in Figure 2E, drifting gratings induced a systematically higher NBG peak frequency compared with static gratings, while still maintaining a monotonic increase with higher contrast levels.

Quantitatively, NBG amplitude increased on average ~57.5% for each contrast level increment in the static grating task and ~29.4% in the drifting grating task, as shown in Table 3. The peak frequency of induced NBG increased on average ~3.7 Hz for each contrast level increment in both the static and the drifting grating tasks (Table 3). However, as noted above, the drifting grating task produced a NBG peak frequency that was on average 7.7 Hz higher than the static task (averaged across subjects who completed both Experiment 1 and 2: N3, N6, N7). We used mixed-effects modeling to evaluate the statistical significance of the effect of contrast (see Materials and Methods and summary in Table 4). Grating stimuli contrast levels significantly modulated NBG amplitude across both experiments (static grating: $p < 0.0001$; drifting grating: $p < 0.0001$). Similar results were found when modeling the peak frequency of NBG (static grating: $p < 0.0001$; drifting grating: $p < 0.0001$). Together, these data show parametric differences in NBG induced by static versus drifting gratings, which are equally well captured by ECoG and sEEG recordings.

While NBG responses are sensitive to the contrast level in both experiments, the peak frequency is further increased by the drifting grating stimuli (i.e., grating motion). To quantify the grating motion effect on NBG responses, we combined data from both experiments and assessed the significance of grating motion effect (drifting versus static). Both the mean log amplitude and peak frequency of induced NBG were significantly

Table 3. Descriptive statistics of mean amplitude and peak frequency of induced NBG in Experiments 1 and 2^a

NBG feature	Task	Contrast level		
		20%	50%	100%
Mean amplitude (% signal change, mean \pm SE)	Static	66.8 \pm 15.2	144.0 \pm 30.0	181.7 \pm 34.6
	Drifting	90.6 \pm 25.8	135.4 \pm 30.4	149.3 \pm 35.2
Peak frequency (Hz, mean \pm SE)	Static	33.7 \pm 0.9	39.0 \pm 1.2	41.0 \pm 1.0
	Drifting	38.7 \pm 0.9	43.8 \pm 0.5	46.1 \pm 0.7

^a Group-averaged NBG amplitudes and peak frequencies for achromatic grating tasks (static/drifting) across contrast levels, using all subjects that participated in each task.

Table 4. Coefficients of fixed parameters in full models and complex models^a

Model components	Coefficients (mean \pm SE)						
	Dependent variable	Fixed effects	Task	$\beta_{\text{intercept}}$	$\beta_{50\%}$	$\beta_{100\%}$	
Mean log amplitude (% signal change)	Contrast	Static	4.3 \pm 0.1	0.6 \pm 0.02	0.8 \pm 0.02		
		Drifting	4.6 \pm 0.2	0.3 \pm 0.01	0.4 \pm 0.01		
	Contrast + motion	Two tasks	4.5 \pm 0.2	0.3 \pm 0.01	0.4 \pm 0.01	0.05 \pm 0.01	
		Contrast	33.8 \pm 1.1	5.2 \pm 0.4	7.2 \pm 0.4		
Peak frequency (Hz)	Contrast	Drifting	38.5 \pm 0.4	5.3 \pm 0.2	7.8 \pm 0.2		
		Two tasks	33.2 \pm 0.3	5.3 \pm 0.2	7.7 \pm 0.2	5.4 \pm 0.2	

^a $\beta_{\text{intercept}}$ captures the 20% contrast level mean in each model. $\beta_{50\%}$ captures the mean difference between 50% and 20% contrast. $\beta_{100\%}$ captures the mean difference between 100% and 20% contrast. β_{motion} captures the mean difference between the drifting and static grating tasks in the complex models.

higher in the drifting grating experiment (Table 4, coefficients β_{motion} ; NBG amplitude: $p < 0.005$; NBG peak frequency: $p < 0.0001$). Considering the mean log amplitude, there was a significant interaction between grating motion and contrast level ($p < 0.0001$) because of an increase in NBG amplitude in response to drifting versus static gratings at low contrast, which was not present for mid-contrast gratings and reversed for high-contrast, where NBG amplitude was smaller for drifting versus static (Fig. 2D). Considering peak frequency, *post hoc* comparisons (see Materials and Methods) confirmed that the NBG peak frequencies were significantly higher in the drifting grating task at each contrast level (all $p < 0.05$ Bonferroni-corrected, p_{corr}). Indeed, the average NBG peak frequency recorded in response to static gratings at 100% contrast was indistinguishable from that of drifting gratings at 20% contrast ($p = 0.49$; Fig. 2E). The above analysis of the drifting grating data averaged responses across trials with different grating orientation and motion directions. Similar results for contrast were found when we considering each motion direction and cardinal orientation separately (see control analysis in Materials and Methods).

NBG displays cardinal orientation selectivity

In quantifying the impact of grating contrast and motion, we collapsed data across different grating orientations. However, intracortical studies in the nonhuman primate have reported orientation tuning of NBG (Berens et al., 2008; Jia et al., 2011). Interestingly, unlike the broad range of orientation preferences observed for spiking and multiunit activity, NBG recorded simultaneously via the local field potential shows a spatially consistent orientation preference (Berens et al., 2008; Jia et al., 2011; Murty et al., 2018; Dubey and Ray, 2020), whereby NBG is turned predominantly to cardinal orientations, in particularly 90° (Murty et al., 2018; Dubey and Ray, 2020). While such a “cardinal bias” has been reported in human visual cortex with neuroimaging (Furmanski and Engel, 2000), the specific orientation tuning properties of NBG have been under examined in the human brain (Self et al., 2016). Therefore, the invasive recordings of the current study provide a unique opportunity to directly test

orientation tuning of NBG in the human brain. We next examined NBG responses across orientations (from 0° to 157.5°, with a 22.5° interval) from the drifting grating task (Experiment 2).

Examination of raw voltage data suggested subtle but consistent modulation of induced oscillations across orientations. As shown in Figure 3A, for an example subject (N7) and electrode, raw voltage responses showed induced oscillations that were more pronounced for the 90° orientation (horizontal). Averaged spectrograms of the same electrode revealed induced oscillations reflected sustained NBG responses, which were relatively higher in amplitude at 90° (Fig. 3B). Examination of the normalized amplitude spectra for each orientation (percentage change of the 250–500 ms poststimulus time window, Fig. 3C) confirmed that NBG amplitude was largest for 90° orientation (polar plot inset shows the NBG preference ~90°, with a circular mean of 80.6°). As shown in Figure 3D, mean normalized NBG amplitude across electrodes and subjects showed a tuning preference for 90° consistently across grating contrast levels. This tuning preference is more clearly observed for the unwrapped orientation tuning plot shown in Figure 3E.

Next, orientation tuning strength and the preferred orientation of each electrode were quantified as the angle and magnitude of the orientation selectivity vector (i.e., the mean vector calculated by mean NBG amplitude across orientations). Across all electrodes, 53.23% showed a 90° preference (defined as the 45° range with 90° as the center, i.e., 67.5°–112.5°, same in the following), with 22.58% showing 0° and 24.19% showing 45° or 135° preference. We further used circular mixed-effect models to evaluate the effect of the contrast level on preferred orientation. The preferred orientation was consistent across contrast levels, as the 95% highest posterior density intervals of the circular means for the three conditions overlap (20% contrast: 58.2°–111.2°; 50% contrast: 51.0°–101.3°; 100% contrast: 68.8°–117.9°). Orientation tuning strength was also consistent across contrast levels (linear mixed-effects model, $p > 0.05$). These findings show a striking consistency with prior local field potential observations in nonhuman primates (Dubey and Ray, 2020), as noted above, and more generally with neuroimaging observations of

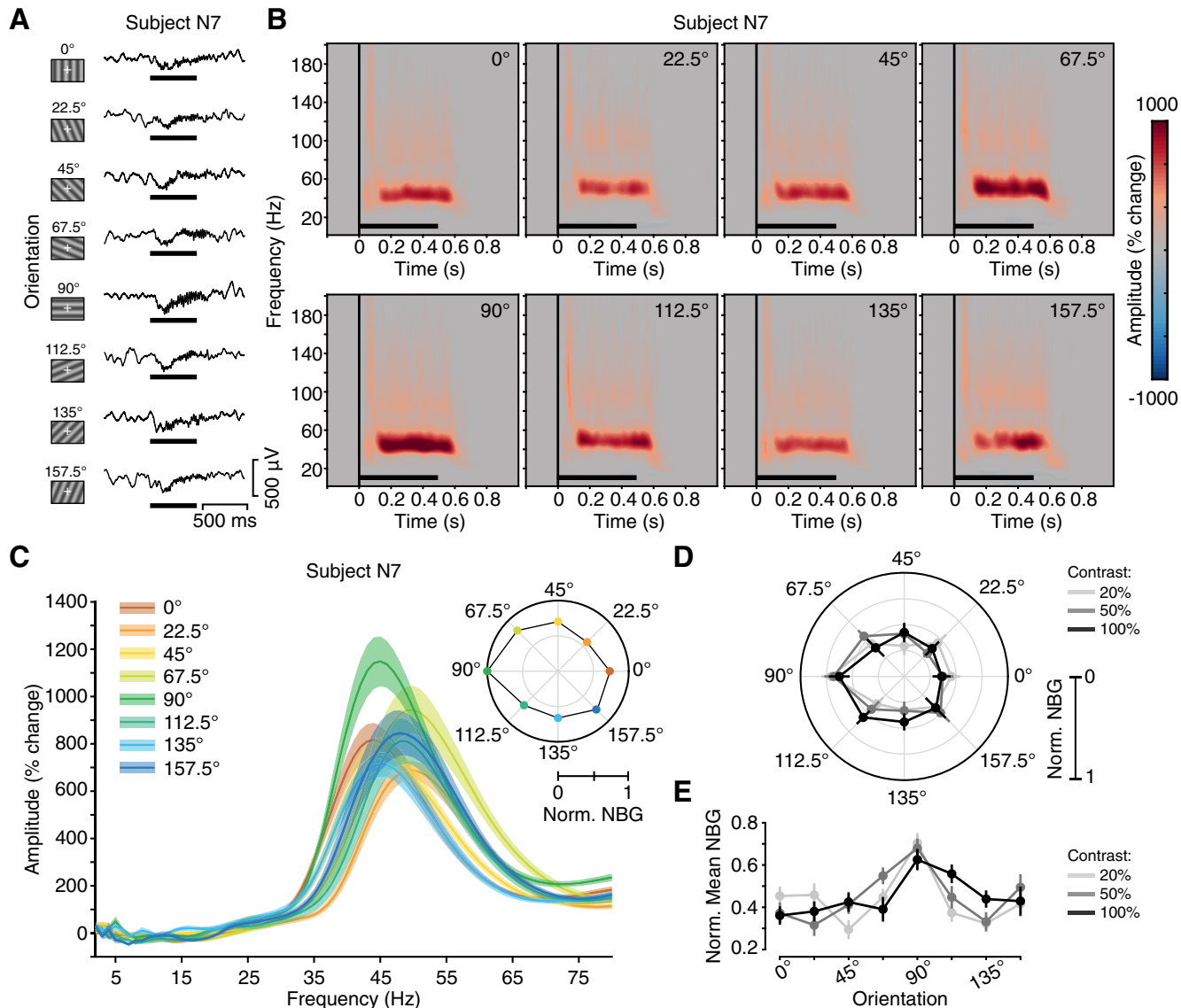


Figure 3. Experiment 2: spectral response to drifting grating orientation. **A**, Example single-trial voltage responses (from Subject N7) for each orientation at 100% contrast level in Experiment 2. Grating stimuli were presented for 500 ms (black horizontal line), with a random ISI of 1.5–2.0 s. **B**, Spectrograms for each orientation from all 100% contrast trials from the same electrode in **A**. Color maps represent percentage change in amplitude relative to the prestimulus period (−500 to 0 ms). Black horizontal line indicates stimulus presentation. **C**, Normalized amplitude spectra for each orientation with the same data in **B**, averaged from the 250–500 ms poststimulus time window. Inset, The normalized mean NBG amplitude of each orientation in polar form of the same data. **D**, Normalized mean NBG amplitude of each orientation for each contrast level in Experiment 2, averaged across all VEP electrodes of Subjects N2–N7 (n elecs = 62). Error bar indicates ± 2 SE. **E**, Same data as in **D**, plotted as unwrapped orientation. **B–E** show that NBG displays an orientation selectivity to 90°.

cardinal biases in human early visual cortex (Furmanski and Engel, 2000).

In addition to orientation, another key feature encoded in early visual cortex is color. As noted above, prior observations in the nonhuman primate have reported that NBG displays chromatic tuning for long wavelength colors (i.e., red/orange) (Shirhatti and Ray, 2018). Recently, we reported that this color tuning of NBG can also be observed in human visual cortex (Bartoli et al., 2019), which was later replicated with noninvasive measurements (Perry et al., 2020). It is therefore of interest to understand how these biases in orientation and color interact to modulate population responses, in particular NBG activity. How these key features of visual cortex selectivity impact NBG activity patterns are critical for understanding its origin and functional significance. Exploring this interaction is further motivated by recent reports showing large-scale organization of single-cell

joint orientation and color tuning in early visual cortex (Garg et al., 2019; Liu et al., 2020). Before examining how color tuning modulates the orientation tuning documented above, we sought to first replicate recent observations of NBG tuning to uniform color stimuli.

NBG displays selectivity to uniform color

To confirm NBG color tuning and ensure it can be observed with penetrating sEEG depth recordings, we replicated the visual color task from Bartoli et al. (2019) in the current study. In Experiment 3 (uniform color task), 5 subjects (N1–N3, N6, N7) were presented full screen uniform colors (9 colors spanning long to short wavelengths, 500 ms duration; see Materials and Methods).

Raw voltage and bandpass NBG voltage traces for example color trials from an sEEG subject (N6) are shown in Figure 4A.

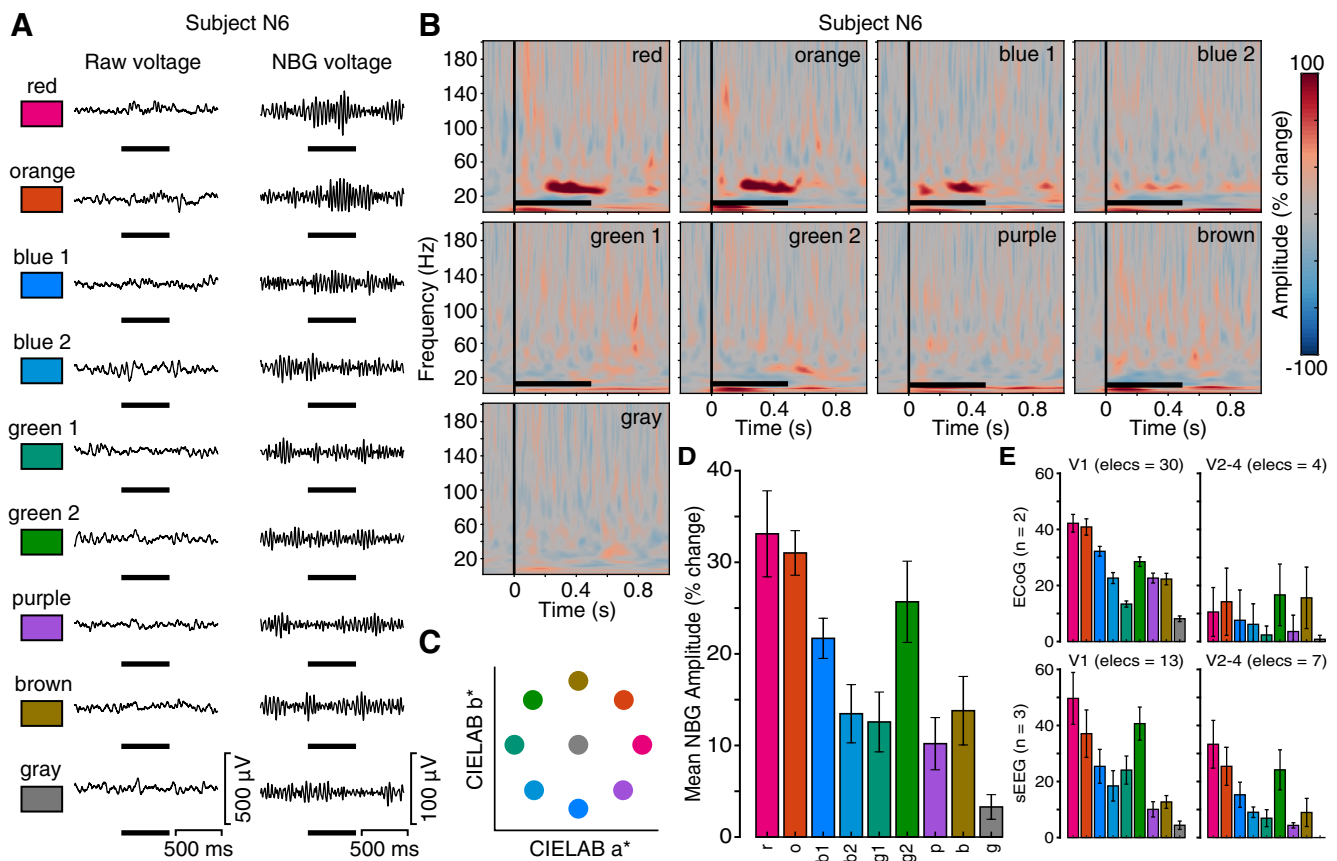


Figure 4. Experiment 3: spectral response to color stimuli. **A**, Example single-trial voltage response (left: raw; right: bandpass NBG range; from Subject N6) for each color (except target color white) in Experiment 3. Full screen uniform colors were presented for 500 ms (black horizontal line), with a random ISI of 1.5–2.0 s. **B**, Spectrogram for each color from all trials from the same electrode used in **A**. Color maps represent percentage change in amplitude relative to the prestimulus period (−500 to 0 ms). Black horizontal line indicates stimulus presentation. **C**, Color location of stimuli in CIE L*a*b* space (lightness plane L = 60). **D**, Group-average mean NBG amplitude response across colors (from Subjects N1–N3, N6, and N7; 250–500 ms time window; error bar indicates ± 1 SE; n elecs = 59). **E**, Data from **D**, separated by electrode type (ECoG/sEEG) and visual area (V1/V2–V4). Responses to red/orange, blue, and green can be consistently observed across electrode types and visual areas, while green responses are relatively higher in sEEG recordings.

Consistent with previous findings (Bartoli et al., 2019), stimulus changes in the raw potential are small in magnitude and difficult to discern. However, when viewing the average spectrograms of the same electrode, clear NBG responses can be observed for red/orange (i.e., long wavelength) and to a lesser extent blue (i.e., short wavelength) hues (Fig. 4B). These findings are consistent with observations of “end spectral” biases in early visual cortex (Nasr and Tootell, 2018), whereby greater neural responses are observed for long (red) and short (blue) wavelengths. Averaging NBG amplitude across all subjects further confirmed the preference for red/orange colors (Fig. 4D). Strikingly, unlike our prior observations, we found the mean amplitude of induced NBG to green was far higher than that of blue at the group level, in part violating an expected end-spectral tuning profile. Nonparametric testing confirmed a significant modulation of NBG amplitude by color (Friedman test of differences: $\chi^2_{(8)} = 29.56$; $p < 0.01$). Post hoc permutation testing confirmed that the NBG amplitude values for red and orange stimuli were all significantly higher than expected by chance (p values < 0.01). Applying permutation testing, all VEP electrodes showed significant NBG responses to either red or orange, 46.9% of electrodes to blue1, and 53.1% to green2 (see Materials and Methods). Across all VEP electrodes, the preferred color was predominately a red hue (red or orange, 82.8%), followed by green hues (green1 or green2, 15.6%) and blue hues (blue1 and blue2, 1.6%). To evaluate whether this unexpected increase in green tuning was dependent on the use of

sEEG electrodes or the visual areas sampled, we plotted the mean NBG amplitude for each color according to electrode type and visual area (Fig. 4E). For sEEG depth electrode recordings, mean NBG amplitude responses are relatively enhanced and more selective for green. To test this, we compared a simple model (NBG responses depending on the color of the stimuli) to a more complex model (NBG responses depending on the color, electrode type, and their interaction). We found that the electrode type had a significant impact on the NBG color tuning profile ($\chi^2_{(10)} = 156.4$; $p < 0.01$). These data suggest a meaningful difference in the color tuning of NBG measured with different electrode types. Another aspect to consider is the presence of a bias for our ECoG electrodes to primarily be within V1 (88%, 30 of 34), compared with sEEG electrodes (65%, 13 of 20). To test whether the visual areas sampled with the different electrodes additionally affected the color tuning, we compared our previous model with a more complex model, including a three-way interaction among electrode type, visual area, and color. We found that adding information on the visual area contributes significantly to the ability of the model to explain the data ($\chi^2_{(20)} = 104.88$; $p < 0.01$). These data suggest that electrode type and electrode visual area are two contributing factors to the more robust responses to green hues reported here.

Related to these observations, it has recently been demonstrated that orientation and color tuning in early visual

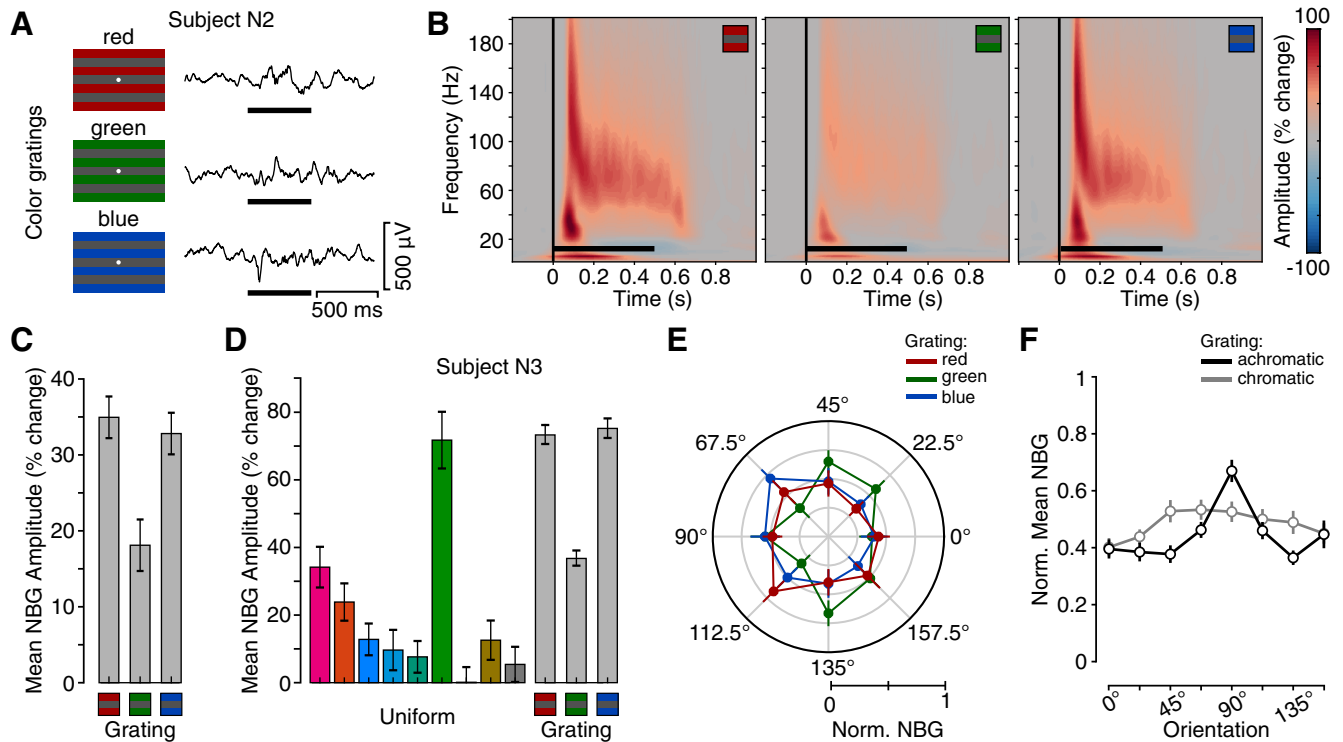


Figure 5. Experiment 4: spectral response to drifting color grating stimuli. **A**, Example single-trial voltage responses (from Subject N2) for each grating color in Experiment 4. Grating stimuli were presented for 500 ms (black horizontal line), with a random ISI of 1.5–2.0 s. **B**, Group-average spectrograms for each grating color (from Subjects N2, N3, N6, and N7; n elecs = 35) in Experiment 4. Color maps represent percentage change in amplitude relative to the prestimulus period (−500 to 0 ms). Black horizontal line indicates stimulus presentation. **C**, Group-average mean NBG amplitude response for color grating task in three color conditions (from Subjects N2, N3, N6, and N7; 250–500 ms time window; error bar indicates ± 1 SE; n elecs = 35). **D**, Mean NBG amplitude response for uniform color task (Experiment 3) and color grating task (Experiment 4) of a VEP electrode with the highest green response of N3 (250–500 ms time window; error bar indicates ± 1 SE), showing how the green response was attenuated when color and orientation were jointly driven, at the single electrode level. **E**, Polar plot of normalized mean NBG amplitude of each orientation for each color condition (averaged across all VEP electrodes of Subjects N2, N3, N6, and N7; n elecs = 35). Error bar indicates ± 2 SE. **F**, Unwrapped orientation tuning plot for normalized mean NBG for Experiment 2 (averaged across contrast conditions; Fig. 3E) and Experiment 3 (averaged across color conditions from E). **B–F** show the interaction between color and orientation in NBG response, such that mid-spectral and cardinal tuning preferences are attenuated when both features were jointly presented.

cortex are more jointly represented than previously appreciated (Garg et al., 2019). Interestingly, these findings suggest a strong representation of red and blue preferring neurons with strong orientation tuning, providing a potential basis to the stimulus dependence of NBG to both grating and chromatic stimuli (Bartoli et al., 2020). As noted above, recent extensions of these findings suggest this strong representation of red/blue is reduced when moving through visual areas V1–V4, such that green becomes more represented and color-selective neurons show more spatial clustering (Liu et al., 2020). Given these joint biases in orientation and color, we would expect interaction effects over NBG modulations when using stimuli driving both stimulus features. To test this, we examined NBG response to colored grating stimuli.

NBG displays color modulation of orientation tuning

To explore the joint orientation-color tuning of NBG, 4 subjects (N2, N3, N6, N7) were presented with full screen chromatic drifting gratings (three colors: red, green, blue; 8 orientations: 0° – 157.5° , with a 22.5° interval; spatial frequency 1 cycle/degree), for a 500 ms duration (Experiment 4, color grating task; see Materials and Methods).

Similar to the responses for uniform color stimuli, chromatic drifting gratings induced relatively modest changes observable in the raw voltage trace (Fig. 5A). Interestingly, group-averaged spectrograms (Fig. 5B) showed NBG responses to each color condition, but with two distinct features. First, responses were

far greater, and approximately similar, for red and blue gratings, in contrast to green, as summarized in Figure 5C. Notably, this effect differs from the response to pure color stimuli where responses to green were greater than blue and approximately similar to red/orange on average. This result is potentially consistent with previous evidence of weaker orientation tuning in green-selective cells (Garg et al., 2019). As an example of this effect, Figure 5D shows the response for the most green-selective electrode observed to uniform color stimuli (Subject N3), which in turn still shows a consistent red/blue bias for drifting color gratings. It is also important to consider that the two greens (green2 in Experiment 3 and green-grating in Experiment 4) have very similar color properties and only a small saturation difference (Table 2), suggesting that the spatial difference between stimuli (uniform color vs presence of orientation information) plays a key role in the NBG response modulation. Second, NBG responses to red and blue are broader in frequency range than that observed for either grating or color stimuli in Experiments 1–3. This broadening of the NBG rhythm further suggests lowered coherence or uniformity in population responses, as well as intertrial variability, likely a consequence of simultaneously driving joint tuning features. These results indicate that the spatial structure of visual stimuli affects the NBG tuning to fundamental visual features (e.g., color), demonstrating the tight interconnection between orientation and color tuning in human early visual areas.

To further investigate how color and orientation tuning interact, we computed group-averaged orientation tuning curves for

each grating color. As shown in Figure 5E, orientation tuning is far less pronounced overall, with no color showing a clear bias for 90° like that observed for achromatic gratings. Rather, for blue gratings, NBG orientation tuning is more pronounced for 67.5°. A similar, yet less strongly tuned, response is also seen for red grating stimuli. In contrast to red and blue, green shows a weaker and reciprocal tuning profile, suggesting another domain of dissociation in population responses. We used the same quantification of orientation tuning as described for the achromatic drifting gratings. Circular mixed-effect model shows that the preferred orientations were not significantly different across three color conditions, as the highest posterior density intervals overlap (red: 77.4°–107.3°; green: 49.7°–100°; blue: 72.5°–100.1°). This may be caused by the relatively small sample size of the current study. In addition, the orientation tuning strength was similar across color conditions (linear mixed-effects model, $p > 0.05$). However, as shown in Figure 5, NBG orientation tuning strength (normalized between 0–1) decreased for color gratings (red = 0.28, green = 0.25, blue = 0.30), compared with achromatic gratings (contrast 20% = 0.36, 50% = 0.37, 100% = 0.35) yielding a significant difference in orientation tuning strength between the two experiments (permutation testing between achromatic and chromatic gratings, $p < 0.001$). Therefore, grating color not only affected the NBG amplitude response but also the orientation tuning profile of NBG, which does not display the same cardinal bias obtained in response to achromatic gratings.

When plotting orientation tuning for achromatic and chromatic gratings together (Fig. 5F), there is a clear loss of the 90° preference present for achromatic gratings, with chromatic gratings showing a flattened tuning. To determine the presence of an interaction between orientation tuning and grating color, we implemented linear mixed-effects model for NBG amplitude by orientation, experiment type (achromatic or color grating), and their interaction. We found a significant interaction term compared with a simpler additive model (i.e., without the interaction term, $\chi^2_{(7)} = 21.74$, $p < 0.01$), demonstrating that NBG orientation tuning is affected by the presence/absence of color information in the oriented gratings.

Together, these findings further support a tight link between the population tuning properties of early visual cortex and the response properties of NBG activity. While NBG reflects known biases for orientation and color, such effects are modulated by their interaction. The differing effects between achromatic and chromatic gratings may be predictive of differential joint tuning biases in population activity, for which recent advances in wide field imaging can examine. As discussed below, these links between ensemble tuning and NBG stimulus dependencies are highly amenable to computational examination and new theoretical views on the functional significance of NBG.

Discussion

Intracranial recordings (ECoG and sEEG) from human visual cortex were used to examine the orientation and color tuning properties of induced NBG oscillations. Consistent with predictions from the nonhuman primate, we observed both orientation and color tuning of NBG to reflect known biases for cardinal orientations (i.e., 90°), and both end- and mid-spectral color ranges (i.e., red/blue and green). We found that these attributes were modulated when orientation and color were jointly driven by colored-grating stimuli. These findings suggest that NBG reflects reverberant population activity dependent on, and sensitivity to, feature selectivity within early visual cortex. Below, we summarize

how these findings relate to recent progress in elucidating the large-scale organization of orientation and color tuning in primate visual cortex and how these stimulus dependencies of visual NBG inform theories of its functional significance.

Before examining orientation tuning, we replicated previous observations of static grating stimuli reliably inducing NBG activity (Ray and Maunsell, 2010; Hadjipapas et al., 2015; Bartoli et al., 2019), whereby NBG peak frequency increased monotonically with higher contrast levels, as did NBG amplitude. Furthermore, we examined how this relationship was modulated by the use of drifting gratings, finding similar contrast effects, but overall faster NBG oscillations. Grating contrast and velocity modulation of NBG peak frequency have previously been observed with both invasive (Jia et al., 2011) and noninvasive (Orekhova et al., 2018) measurements, adding to other stimulus features which modulate the frequency of visually induced γ rhythms. These observations suggest that NBG occurs for specific stimulus configurations with high-contrast edge/grating features intersecting the RF (Vinck and Bosman, 2016; Hermes et al., 2019; Bartoli et al., 2020). Given the strong selectivity in early visual cortex for such features, it is important to examine how stimulus orientation modulates NBG activity.

Using drifting grating stimuli, we observed NBG amplitude to be biased for horizontally oriented gratings (90°). This preference for a specific orientation seems unexpected for a population-level signal, such as NBG, which captures the summed activity of local ensembles with diverse orientation preferences. Interestingly, prior evidence from human neuroimaging studies has shown a cardinal bias in population measures of orientation tuning (Furmanski and Engel, 2000; Sun et al., 2013), such that responses are more attenuated for oblique angles. This vertical/horizontal orientation bias has also been well known in psycho-physical performance (Wilson and Giese, 1977). Furthermore, work in the nonhuman primate has also reported a cardinal bias of visual NBG, specifically for 90° orientations (Murty et al., 2018; Dubey and Ray, 2020). More generally, these studies have shown that NBG displays consistent and spatially coherent tuning for a single orientation across proximal recordings sites, despite the underlying spiking activity showing diverse tuning profiles (Berens et al., 2008; Jia et al., 2011; Murty et al., 2018). Indicative of this NBG tuning reflecting larger-scale population biases, reduced stimulus size (i.e., smaller population activated) greatly reduces the strength and specificity of NBG orientation preference (Jia et al., 2011). Together, these observations suggest that visual NBG in humans displays a cardinal orientation bias similar to other neural population-level measures in humans and nonhuman primates. However, orientation is not the only key stimulus feature encoded in early visual cortex; color is also strongly represented and has recently been linked to NBG tuning.

Recent work in nonhuman primates has demonstrated color tuning for NBG, being particularly enhanced for long wavelength (i.e., red/orange), and to a lesser extent, short wavelength colors (i.e., blue) (Shirhatti and Ray, 2018). We recently replicated this NBG color tuning via invasive recordings in human visual cortex (Bartoli et al., 2019), with similar findings subsequently shown via noninvasive measurements (Perry et al., 2020). Similar to orientation, this color tuning of NBG is consistent with prior neuroimaging reports of an end-spectral bias in population responses within human early visual cortex, particularly V1 (Nasr and Tootell, 2018), with larger hemodynamic responses for long and short wavelength colors. In the present study, we observed a similar influence of color, where NBG responses were largest for red

and orange hues. However, unlike our prior work, we observed a larger response to green than blue, which is inconsistent with an end-spectral bias.

What might account for this difference between studies? Regarding stimuli, subjects were presented with the same stimuli via the same apparatus, ruling out this experimental confound. One key difference is the predominate use of sEEG depth recordings in the current study. Penetrating depth electrodes differ in their physical structure, trajectory through the parenchyma, and proximity to gray matter, all impacting recorded signals. For example, unlike surface ECoG arrays, sEEG depth electrodes may contact the sulcal wall and fundus, with differing positions relative to the cortical layers and to the 3D topology of visual cortex. Indeed, penetrating electrodes may collect signals not only from different cell bodies but also from the axons that provide input and output from that area. We therefore suspect that the sEEG recordings in the present study allowed for capturing the previously observed end-spectral hue bias in addition to green hue bias. Indeed, mean NBG amplitude responses were relatively enhanced and more selective for green considering sEEG recordings. Another factor is the color space employed, which can influence the relative strength of red/orange tuning (Stauch et al., 2021). Future studies using full retinotopic identification of the visual areas are necessary to disentangle the relationship between NBG tuning profile, visual area sampling, and electrode features.

Overall, color tuning of NBG, and its potential variation across visual area, follows a similar relationship to orientation. While red, green, and blue selectivity can be observed in early visual cortex, recent findings in wide field imaging have shown a large predominance of red and blue preferring cells in macaque V1 (Garg et al., 2019; Liu et al., 2020). Again, this predominance at the cellular level links to the population tuning properties exhibited by NBG activity. In addition, red/blue predominance found in V1 changes progressively into downstream visual areas V2-V4, such that the density of green preferring cells increases and that cells sharing the same color preference are more spatially clustered (Liu et al., 2020). Together, these attributes speak to the NBG tuning we observed, which can be considered as a coarse summated sampling of these different populations. Critically, recent observations of joint color and orientation tuning (Garg et al., 2019) suggest partially overlapping circuits driving population-level activity in response to these stimulus features (Bartoli et al., 2020). With this unique intersection in mind, we examined the influence of joint orientation and color tuning of NBG activity.

Color-grating (red, green, blue) stimuli were used to examine how joint driving of orientation and color influenced the NBG activity observed for orientation and color independently. Interestingly, we observed three clear departures from our first set of observations. First, induced NBG was on average broader in its frequency (see Fig. 5*B*). Second, NBG responses were approximately similar for both red and blue, and comparatively reduced for green, which differs from the clear preferences observed for uniform colors. Third, color-gratings did not drive similar cardinal orientation tuning like achromatic gratings and orientation tuning strength was overall reduced.

What factors can account for these differences? By driving both orientation and color stimulus features, one may expect less coherent population-level activity (i.e., only specific subpopulations are selectively driven), which is in part supported by the lower overall amplitude of NBG responses to chromatic versus achromatic gratings. A similar intuition may speak to the broadening of induced NBG frequency. Regarding specific color

effects, the reduced responsiveness to green stimuli (when presented as gratings) may be accounted for by prior evidence of weaker orientation tuning for green preferring cells, compared with red and blue (Garg et al., 2019). Future studies are needed to examine how cell tuning properties shift over visual areas, for both color preferences and joint color-orientation effects. Based on our data and the interpretation of the observed effects, we would expect reduced evidence for cardinal biases when driving specific color channels.

NBG oscillations are a striking feature of stimulus induced responses in visual cortex. This high-frequency rhythm has been the subject of great interest in theories of visual perception and cognition more broadly. As a periodic modulator of neural excitability, NBG activity is an appealing mechanism for synchronizing neural dynamics. One challenge for such a mechanism is generalization to the rich array of sensory inputs. While classic grating stimuli are highly effective at driving NBG responses, the induced amplitude and frequency of NBG are particularly sensitive to all attributes of such stimuli (e.g., grating size, contrast, spatial frequency, velocity, uniformity). Given that all of these parameters dynamically change during natural vision, theories suggesting that NBG synchrony supports perception and intra-areal communication must account for continuous changes in magnitude and frequency driven by a host of stimulus dependencies. These challenges grow with consideration of chromatic modulation of NBG properties. In contrast, new hypotheses are emerging, linking NBG occurrence to the presence of specific feature configurations in the visual input able to provoke rhythmic circuit dynamics (Hermes et al., 2019; Peter et al., 2019; Bartoli et al., 2020; Uran et al., 2020). Computational models will need to account for the diverse parametric relationships between lower-level stimulus features and NBG responses (Heeger and Zemlianova, 2020). Importantly, new theories are needed to help establish general rules of how stimulus composition modulates NBG activity during natural vision (Hermes et al., 2019; Uran et al., 2020). Improved computational and experimental links between stimuli, visual circuit properties and the γ rhythm are critical for elucidating its functional significance.

References

- Bartoli E, Bosking W, Chen Y, Li Y, Sheth SA, Beauchamp MS, Yoshor D, Foster BL (2019) Functionally distinct gamma range activity revealed by stimulus tuning in human visual cortex. *Curr Biol* 29:3345–3358.e3347.
- Bartoli E, Bosking W, Foster BL (2020) Seeing visual gamma oscillations in a new light. *Trends Cogn Sci* 24:501–503.
- Bates D, Maechler M, Bolker B, Walker S, Christensen RH, Singmann H, Dai B (2014) lme4: linear mixed-effects models using Eigen and S4 (version 1.1-7). Available at <https://cran.r-project.org/web/packages/lme4/index.html>.
- Bates D, Machler M, Bolker BM, Walker SC (2015) Fitting linear mixed-effects models using lme4. *J Stat Softw* 67:1–48.
- Berens P, Keliris GA, Ecker AS, Logothetis NK, Tolias AS (2008) Comparing the feature selectivity of the gamma-band of the local field potential and the underlying spiking activity in primate visual cortex. *Front Syst Neurosci* 2:2.
- Bosking WH, Sun P, Ozker M, Pei X, Foster BL, Beauchamp MS, Yoshor D (2017) Saturation in phosphene size with increasing current levels delivered to human visual cortex. *J Neurosci* 37:7188–7197.
- Brainard DH (1997) The Psychophysics Toolbox. *Spat Vis* 10:433–436.
- Brunet N, Bosman CA, Roberts M, Oostenveld R, Womelsdorf T, De Weerd P, Fries P (2015) Visual cortical gamma-band activity during free viewing of natural images. *Cereb Cortex* 25:918–926.
- Brunet N, Vinck M, Bosman CA, Singer W, Fries P (2014) Gamma or no gamma, that is the question. *Trends Cogn Sci* 18:507–509.
- Buzsaki G, Wang XJ (2012) Mechanisms of gamma oscillations. *Annu Rev Neurosci* 35:203–225.

- Buzsaki G, Logothetis N, Singer W (2013) Scaling brain size, keeping timing: evolutionary preservation of brain rhythms. *Neuron* 80:751–764.
- Cremers J (2020) bpnreg: Bayesian Projected Normal Regression Models for Circular Data. R package version 2.0.1. Available at <https://CRAN.R-project.org/package=bpnreg>.
- Cremers J, Klugkist I (2018) One direction? a tutorial for circular data analysis using R with examples in cognitive psychology. *Front Psychol* 9:2040.
- Dale AM, Fischl B, Sereno MI (1999) Cortical surface-based analysis: I. Segmentation and surface reconstruction. *Neuroimage* 9:179–194.
- Dubey A, Ray S (2020) Comparison of tuning properties of gamma and high-gamma power in local field potential (LFP) versus electrocorticogram (ECoG) in visual cortex. *Sci Rep* 10:5422.
- Economides JR, Sincich LC, Adams DL, Horton JC (2011) Orientation tuning of cytochrome oxidase patches in macaque primary visual cortex. *Nat Neurosci* 14:1574–1580.
- Fries P (2009) Neuronal gamma-band synchronization as a fundamental process in cortical computation. *Annu Rev Neurosci* 32:209–224.
- Fries P (2015) Rhythms for cognition: communication through coherence. *Neuron* 88:220–235.
- Fries P, Nikolic D, Singer W (2007) The gamma cycle. *Trends Neurosci* 30:309–316.
- Fries P, Scheeringa R, Oostenveld R (2008) Finding gamma. *Neuron* 58:303–305.
- Furmanski CS, Engel SA (2000) An oblique effect in human primary visual cortex. *Nat Neurosci* 3:535–536.
- Garg AK, Li P, Rashid MS, Callaway EM (2019) Color and orientation are jointly coded and spatially organized in primate primary visual cortex. *Science* 364:1275–1279.
- Gieselmann MA, Thiele A (2008) Comparison of spatial integration and surround suppression characteristics in spiking activity and the local field potential in macaque V1. *Eur J Neurosci* 28:447–459.
- Groppe DM, Bickel S, Dykstra AR, Wang X, Megevand P, Mercier MR, Lado FA, Mehta AD, Honey CJ (2017) iELVis: an open source MATLAB toolbox for localizing and visualizing human intracranial electrode data. *J Neurosci Methods* 281:40–48.
- Hadjipapas A, Lowet E, Roberts MJ, Peter A, De Weerd P (2015) Parametric variation of gamma frequency and power with luminance contrast: a comparative study of human MEG and monkey LFP and spike responses. *Neuroimage* 112:327–340.
- Heeger DJ, Zemlianova KO (2020) A recurrent circuit implements normalization, simulating the dynamics of V1 activity. *Proc Natl Acad Sci USA* 117:22494–22505.
- Henriksson L, Nurminen L, Hyvarinen A, Vanni S (2008) Spatial frequency tuning in human retinotopic visual areas. *J Vis* 8:5–13.
- Hermes D, Miller KJ, Wandell BA, Winawer J (2015a) Gamma oscillations in visual cortex: the stimulus matters. *Trends Cogn Sci* 19:57–58.
- Hermes D, Miller KJ, Wandell BA, Winawer J (2015b) Stimulus dependence of gamma oscillations in human visual cortex. *Cereb Cortex* 25:2951–2959.
- Hermes D, Petridou N, Kay K, Winawer J (2019) An image-computable model for the stimulus selectivity of gamma oscillations. *bioRxiv* 583567.
- Jenkinson M, Beckmann CF, Behrens TE, Woolrich MW, Smith SM (2012) FSL. *Neuroimage* 62:782–790.
- Jia X, Smith MA, Kohn A (2011) Stimulus selectivity and spatial coherence of gamma components of the local field potential. *J Neurosci* 31:9390–9403.
- Kayser C, Kim M, Ugurbil K, Kim DS, Konig P (2004) A comparison of hemodynamic and neural responses in cat visual cortex using complex stimuli. *Cereb Cortex* 14:881–891.
- Kayser C, Salazar RF, Konig P (2003) Responses to natural scenes in cat V1. *J Neurophysiol* 90:1910–1920.
- Leventhal AG, Thompson KG, Liu D, Zhou Y, Ault SJ (1995) Concomitant sensitivity to orientation, direction, and color of cells in layers 2, 3, and 4 of monkey striate cortex. *J Neurosci* 15:1808–1818.
- Liu Y, Li M, Zhang X, Lu Y, Gong H, Yin J, Chen Z, Qian L, Yang Y, Andolina IM, Shipp S, McLoughlin N, Tang S, Wang W (2020) Hierarchical representation for chromatic processing across macaque V1, V2, and V4. *Neuron* 108:538–550.e535.
- Murty D, Shirhatti V, Ravishankar P, Ray S (2018) Large visual stimuli induce two distinct gamma oscillations in primate visual cortex. *J Neurosci* 38:2730–2744.
- Nasr S, Tootell RB (2018) Columnar organization of mid-spectral and end-spectral hue preferences in human visual cortex. *Neuroimage* 181:748–759.
- Orekhova EV, Sysoeva OV, Schneiderman JF, Lundstrom S, Galuta IA, Goiaeva DE, Prokofyev AO, Riaz B, Keeler C, Hadjikhani N, Gillberg C, Stroganova TA (2018) Input-dependent modulation of MEG gamma oscillations reflects gain control in the visual cortex. *Sci Rep* 8:8451.
- Papademetris X, Jackowski MP, Rajeevan N, DiStasio M, Okuda H, Constable RT, Staib LH (2006) BioImage Suite: an integrated medical image analysis suite: an update. *Insight J* 2006:209.
- Perry G, Taylor NW, Bothwell PC, Milbourn CC, Powell G, Singh KD (2020) The gamma response to colour hue in humans: evidence from MEG. *PLoS One* 15:e0243237.
- Peter A, Uran C, Klon-Lipok J, Roese R, van Stijn S, Barnes W, Dowdall JR, Singer W, Fries P, Vinck M (2019) Surface color and predictability determine contextual modulation of V1 firing and gamma oscillations. *Elife* 8:e42101.
- R Development Core Team (2010) R: a language and environment for statistical computing. Vienna: R foundation for Statistical Computing.
- Ray S, Maunsell JH (2010) Differences in gamma frequencies across visual cortex restrict their possible use in computation. *Neuron* 67:885–896.
- Ray S, Maunsell JH (2011) Different origins of gamma rhythm and high-gamma activity in macaque visual cortex. *PLoS Biol* 9:e1000610.
- Ray S, Maunsell JH (2015) Do gamma oscillations play a role in cerebral cortex? *Trends Cogn Sci* 19:78–85.
- Rosenke M, Weiner KS, Barnett MA, Zilles K, Amunts K, Goebel R, Grill-Spector K (2018) A cross-validated cytoarchitectonic atlas of the human ventral visual stream. *Neuroimage* 170:257–270.
- Self MW, Peters JC, Possel JK, Reithler J, Goebel R, Ris P, Jeurissen D, Reddy L, Claus S, Baayen JC, Roelfsema PR (2016) The effects of context and attention on spiking activity in human early visual cortex. *PLoS Biol* 14:e1002420.
- Shirhatti V, Ray S (2018) Long-wavelength (reddish) hues induce unusually large gamma oscillations in the primate primary visual cortex. *Proc Natl Acad Sci USA* 115:4489–4494.
- Shirhatti V, Ravishankar P, Ray S (2020) Gamma oscillations in primate primary visual cortex are severely attenuated by small stimulus discontinuities. *bioRxiv*. doi:<https://doi.org/10.1101/2020.07.19.210922>.
- Stauch BJ, Peter A, Ehrlich I, Nolte Z, Fries P (2021) Human visual gamma for color stimuli: When LGN drive is equalized, red is not special. *bioRxiv*. doi:<https://doi.org/10.1101/2021.11.22.469550>.
- Sun P, Gardner JL, Costagli M, Ueno K, Waggoner RA, Tanaka K, Cheng K (2013) Demonstration of tuning to stimulus orientation in the human visual cortex: a high-resolution fMRI study with a novel continuous and periodic stimulation paradigm. *Cereb Cortex* 23:1618–1629.
- Uran C, Peter AS, Lazar A, Barnes W, Klon-Lipok J, Shapcott KA, Roese R, Fries P, Singer W, Vinck M (2020) Predictive coding of natural images by V1 activity revealed by self-supervised deep neural networks. *bioRxiv*. doi:<https://doi.org/10.1101/2020.08.10.242958>.
- Vinck M, Bosman CA (2016) More gamma more predictions: gamma-synchronization as a key mechanism for efficient integration of classical receptive field inputs with surround predictions. *Front Syst Neurosci* 10:35.
- Wilson HR, Giese SC (1977) Threshold visibility of frequency gradient patterns. *Vision Res* 17:1177–1190.
- Yoshor D, Bosking WH, Ghose GM, Maunsell JH (2007) Receptive fields in human visual cortex mapped with surface electrodes. *Cereb Cortex* 17:2293–2302.